Surface structural phase transition induced by the formation of metal-organic networks on Si(111)-$\sqrt{7} \times \sqrt{3}$-In surface

T. Suzuki,[a,b] J. Lawrence,[b] J. M. Morbec,[c] P. Kratzer,[c] G. Costantini[b]

[a]*Department of Electronics Engineering and Computer Science, Fukuoka University, Fukuoka 814-0180, Japan*

[b]*Department of Chemistry, University of Warwick, Coventry, CV4 7AL, United Kingdom*

[c]*Faculty of Physics, University of Duisburg-Essen, Lotharstrasse 1, 47057 Duisburg, Germany*

Abstract

We study the adsorption of 7,7,8,8-tetracyanoquinodimethane (TCNQ) on the Si(111)-$\sqrt{7} \times \sqrt{3}$-In surface, a known surface superconductor. Scanning tunneling microscopy shows the development of a surface-confined metal organic network (SMON) where TCNQ molecules coordinate with indium atoms from the underlying $\sqrt{7} \times \sqrt{3}$ reconstruction. The formation of the SMON causes a surface structural phase transition from the $\sqrt{7} \times \sqrt{3}$ to a previously unknown 5 × 5 reconstruction of the Si(111)-In surface. Scanning tunneling spectroscopy measurements indicate that the 5 × 5 reconstruction has a stronger insulating character than the $\sqrt{7} \times \sqrt{3}$ reconstruction. Density-functional-theory calculations are used to evaluate the atomic arrangement and stability of the 5 × 5 and $\sqrt{7} \times \sqrt{3}$ reconstructions as a function of In coverage, and suggest that the structural phase transition is driven by a slight reduction of the In coverage, caused by the incorporation of indium atoms into the SMON.

†Electronic supplementary information (ESI) available. See DOI:

Introduction

Atomically-thin metal layers adsorbed on the Si(111) surface, such as Si(111)-$\sqrt{7} \times \sqrt{3}$-In and Si(111)-$\sqrt{7} \times \sqrt{3}$-Pb surfaces, were recently found to be surface superconductors at 1-3 K.[1-5] With respect to their bulk counterparts, surface superconductors have the unique advantage that their superconducting states are very sensitive to adsorption of atoms or molecules, a property that can be utilized to control and finely tune their superconductivity. So far, it has been demonstrated that the adsorption of Mn- and fluorinated Cu-phthalocyanines on the Si(111)-$\sqrt{7} \times \sqrt{3}$-In surface shifts its superconducting transition temperature (T_c) to lower values, while that of Cu-phthalocyanine shifts T_c to higher values, which was attributed to the directionality of the relevant *d*-orbitals and to a hole doping by extraction of surface electrons.[6,7]

Surface-confined metal organic networks (SMONs) have also been investigated extensively on various solid surfaces, because of their potential in applications for heterogeneous catalysis, sensing, proton conductors, gas storage and separation.[8] SMONs are compounds with a regular two-dimensional reticular structure consisting of metal atoms (typically in a cationic charge state) coordinated to organic ligands (typically in an anionic charge state). In particular, 7,7,8,8-tetracyanoquinodimethane (TCNQ) is an organic ligand frequently used to fabricate SMONs, as well as three-dimensional bulk metal organic frameworks.[9,10] TCNQ is also known to be a strong organic electron acceptor and has been used to synthesize organic conductors in the form of charge-transfer complexes with various molecular electron acceptors.[11] So far it has been reported that TCNQ molecules adsorbed on various noble metal surfaces can form SMONs together with Ni,[12, 13, 14] Mn,[14, 15] Cs,[15] Na,[16, 17] K,[18] Ag,[19] and Au atoms.[20] Moreover, the metal centers embedded in the Ni-TCNQ and the Mn-TCNQ SMONs showed ferromagnetic and antiferromagnetic coupling, respectively,[13,14] while a Kondo effect was observed in the Na-TCNQ SMON.[17]

In the present study, we have investigated the TCNQ adsorption on the Si(111)-$\sqrt{7} \times \sqrt{3}$-In surface by scanning tunneling microscopy (STM) and scanning tunneling spectroscopy (STS). We found that In-TCNQ SMONs form on the Si(111)-In surface and that their development causes a surface structural phase transition from the $\sqrt{7} \times \sqrt{3}$ to a previously unknown 5 × 5 reconstruction. The atomic arrangement and stability of the 5 × 5 and $\sqrt{7} \times \sqrt{3}$ reconstructions with several different In coverages were investigated using first-principles density functional theory (DFT) calculations. On the basis of these theoretical results, we assign the surface structural phase transition to a reduction of the In coverage, caused by the incorporation of indium atoms into the SMONs.

Experimental Methods

A detailed description of the experimental methods is given in reference.[21] Briefly, the Si samples were cut out from a *n*-type phosphorus-doped Si(111) wafer (0.007-0.013 Ω cm, Siltronix). The Si samples were flashed to 1200-1250 ºC several times in ultra-high vacuum (UHV), in order to obtain the clean 7×7 reconstruction. Indium (shot, 1-3 mm, 99.9999 %, Matek) was fixed by melting onto a tungsten filament and then sublimed by heating the tungsten filament by direct current onto the Si substrates. During deposition the Si substrate was held at room temperature (RT), and the samples were successively heated for 1-10 s up to 500 ºC in order to obtain the $\sqrt{7} \times \sqrt{3}$ reconstruction. Finally, the TCNQ molecules were deposited by organic molecular beam epitaxy onto the Si substrates held at RT.

The STM images were acquired at 77 K in UHV using chemically etched tungsten tips. *dI*/*dV* spectroscopy was performed by adding a sinusoidal modulation voltage (typical amplitude 10 mV and frequency 3.1 kHz) to the bias voltage via an lock-in amplifier and recording the output of the lock-in tuned on the first harmonic.

Computational Methods

First-principles calculations were performed in the framework of DFT,[22] as implemented in the FHI-aims code,[23] an all-electron full-potential code with numeric atom-centered basis functions. The generalized gradient approximation (GGA) proposed by Perdew, Burke, and Ernzerhof (PBE)[24] was employed for the exchange-correlation functional; due to large size of the investigated systems, we used "light" basis sets with "tier 2," "tier 3," and "tier 2" sets for In, Si, and H, respectively. Since the $\sqrt{7} \times \sqrt{3}$ and 5 × 5 reconstructions are commensurate with each other (see Fig. 2), we simulated both of them by using a (5 × 5) surface unit cell; five Si bilayers and a vacuum region of approximately 30 Å were used to build the slab within the supercell approach. Two layers of In atoms were adsorbed on the front side of the slab while hydrogen atoms were employed to passivate the rear side of the slab. During structural relaxations, the bottom Si bilayer was constrained to the bulk position, whereas the remaining four Si bilayers as well as the In atoms were allowed to relax; we considered a convergence criterion of 1×10^{-2} eV/ Å for the maximum residual force component per atom. The Brillouin zone

was sampled with a 5×5×1 Monkhorst-Pack[25] k-point grid.

In the results section, we report the formation energies of several atomic configurations investigated in the present study. For this we define the formation energy E_f as

$$E_f = E_{\mathrm{In}/Si(111)} - E_{Si(111)} - N \cdot E_{\mathrm{In}}$$

where $E_{\mathrm{In}/Si(111)}$ and $E_{Si(111)}$ are the total energies of the Si(111)–5 × 5–In and of an unreconstructed, but relaxed Si(111) slab with the same surface area, E_{In} is the energy of the bulk In in the face-centered tetragonal structure and N is the number of In atoms in the system.

Results

Figures 1(a) and 1(b) show typical STM images before and after the TCNQ deposition on the Si(111)-$\sqrt{7} \times \sqrt{3}$-In surface, respectively. Before molecular deposition, the $\sqrt{7} \times \sqrt{3}$ reconstruction is characterized by many irregular-shaped holes – one of which is indicated by a red arrowhead in the upper side of Fig. 1(a) – as has been reported previously in the literature (for example, compare with Fig. 3(a) in reference[21] or Fig. 1(d) in reference[26]). As a result of the threefold rotational symmetry of the Si(111) surface, the $\sqrt{7} \times \sqrt{3}$ reconstruction displays three equivalent domains rotated with respect to each other by 120 °, as indicated by three red dotted lines in the upper side of Fig. 1(a). Upon deposition, the TCNQ molecules form an ordered structure that will later be proven to be a SMON with indium atoms taken from the underlying $\sqrt{7} \times \sqrt{3}$ reconstruction, as indicated in the upper right corner of Fig. 1(b). The SMON islands are sparsely distributed on the surface, usually have irregular shapes, and their size is in the 30 - 100 nm range. Interestingly, on the terrace where the SMON is formed, the surface reconstruction changes from $\sqrt{7} \times \sqrt{3}$ to a new reconstruction with a 5×5 symmetry; this corresponds the large bright region in the center of Fig. 1(b). It should be noted that, depending on the indium coverage and on the temperature of a subsequent annealing, the adsorption of indium onto the Si(111) surface has been shown to produce various reconstructions, such as the $\sqrt{3} \times \sqrt{3}$, $\sqrt{31} \times \sqrt{31}$, 4×1, 2×2 and the $\sqrt{7} \times \sqrt{3}$,[27,28] but that no reconstruction with a 5×5 symmetry has so far been reported. Some substrate regions retain the $\sqrt{7} \times \sqrt{3}$ reconstruction also after the molecular deposition (e.g. see the lower part of Fig. 1(b)) and

the TCNQ molecules adsorb also on these areas though there they form only disordered islands, as indicated by a red arrowhead. There is usually an apparent height difference of about 0.25 nm between the $\sqrt{7} \times \sqrt{3}$ and the 5 × 5 terraces (see Fig. S1 of the ESI†), although in some exceptional cases almost no height difference exists between them

Figure 1(c) shows an enlarged STM image of the ordered TCNQ structures. Each TCNQ molecule displays a characteristic intramolecular contrast consisting of a nodal central plane separating two symmetric striped features with a central circular protrusion; one of them has been highlighted by a white dashed circle and has been reproduced at a higher contrast in the lower left part of Fig. 1(c). This shape closely resembles that of the lowest unoccupied molecular orbital (LUMO) of an isolated TCNQ molecule as calculated by DFT (e.g. compare with Fig. 1b of reference[29]), or the STM-measured shape of an adsorbed TCNQ molecule that is negatively charged (compare for example with Fig.7b of reference[30] or with Fig. 4c of reference[20]). The appearance of these "LUMO-shaped" features at negative sample bias (i.e. for filled sample states) indicates that the TCNQ molecules in the ordered structure must be negatively charged. This is the expected charging state of TCNQ in coordination complexes with metal atoms.[16,18,19,31,32]

The arrangement of the TCNQ molecules inside the ordered structure is clearly seen in the area indicated by a white dashed rectangle towards the top of Fig. 1(c) (and even better in the corresponding higher contrast inset). Each TCNQ molecule is oriented perpendicular to the four neighboring molecules, forming a windmill-like motif. A schematic molecular model of this arrangement is shown in the bottom-right inset of Fig. 1(c), where carbon, nitrogen and hydrogen atoms are depicted as grey, blue and white spheres, respectively. The model also assume that indium metal centers – shown as green spheres – exist at the position close to the four cyano groups of the four TCNQ molecules that compose a windmill. The STM images reveal a protrusion in correspondence with this specific position, as indicated by the green dotted circle in the central high-contrast inset of Fig. 1(c). An analogous molecular arrangement has been reported for the *α* phase of the Ni-TCNQ SMON formed on the Ag(100) surface (denoted as SMON(α) hereafter),[12] as well as for the Na-TCNQ SMON on Au(111),[16,17] and the K-TCNQ SMON on Ag(111).[18] Based on these similarities, the ordered structure in Fig. 1(c) is considered to be the In-TCNQ SMON(α).

Several very bright humps are also seen in Fig. 1(c), one of which is indicated by a black dashed circle in the upper left corner (it should be noted that their lateral size is significantly increased by the high contrast used for representing the STM image). These humps seem to be located in correspondence to the indium centers in the SMON(α)

and they appear to be mobile, disappearing and reappearing in between successive STM scans (See Fig. S2 in the ESI†). We are not able to precisely identify them but, based on their mobility and on the absence of any finer inner structure in the STM images, we suggest that they might be second layer indium adatoms.

Figure 1(d) shows an enlarged STM image of a bare 5 × 5 reconstructed terrace close to a region with the SMON(α) (this latter is barely visible because of the high contrast needed to visualize the details of the 5 × 5 reconstruction). A section of the 5 × 5 area indicated by a white dashed rectangle has been reproduced at a higher contrast in the right part of Fig. 1(d). A white dashed parallelogram inside the inset indicates the 5 × 5 unit cell, while a white dashed circle in the upper left part of the image highlights an isolated TCNQ molecule. This latter has a markedly different appearance with respect to the TCNQ molecules within the SMON(α), with its center not showing any nodal plane but rather a region of higher intensity. This shape closely resembles that of the highest occupied molecular orbital (HOMO) of an isolated TCNQ molecule as calculated by DFT (compare with Fig.1b of reference[29]), or the STM appearance of a neutral adsorbed TCNQ molecule (compare with Fig.2a of reference[29] or Fig.6b of reference[30]). Since Fig. 1(d) was acquired at negative sample bias (i.e. for filled sample states), this observation indicates that on the 5 × 5 terraces isolated TCNQ molecule must be in a neutral charge state. This is further evidence that only within the SMON(α) structures do the TCNQ molecules get negatively charged, as a result of their coordination with In atoms and the ensuing charge transfer. A fast Fourier transform pattern generated from a STM image of a wide 5 × 5 region is shown in the inset of Fig. 1(d), which clearly shows spots caused by the 5 × 5 periodicity (indicated by six cyan circles and the corresponding label), in addition to the fundamental 1 × 1 spots (indicated by a yellow circle and the corresponding label).

Figure 2 shows a schematic drawing of a bulk terminated Si(111) surface, where Si atoms are indicated by dark yellow spheres (only the topmost bilayer is drawn in the figure). The 5 × 5 and $\sqrt{7} \times \sqrt{3}$ periodicities are indicated by red and blue unit cells,

respectively and the schematic clearly shows that they are commensurate to each other, with the former having a five times larger area than the latter. Therefore, the 5 × 5 reconstruction observed in the present study can be regarded as a superstructure of the $\sqrt{7} \times \sqrt{3}$ reconstruction.

Figure 3 shows STM images of the 5 × 5 reconstruction taken at the same sample position with six different sample-bias voltages, from –2.0 V to +2.0 V. A white dotted parallelogram in Figs. 3(a) and 3(f) and a white solid one in Fig. 3(a) indicate the unit cells of the 5 × 5 and the $\sqrt{7} \times \sqrt{3}$ reconstructions, respectively. A contaminant is indicated by white dashed circles in the center of the images and acts as a position marker. The appearance of the 5 × 5 reconstruction is significantly different from that of the $\sqrt{7} \times \sqrt{3}$ reconstruction, as can be directly verified by comparison with Fig. 1(a) of this present paper and Fig. 3 of reference.[21] Irrespectively of the bias voltage, there is no trace of the $\sqrt{7} \times \sqrt{3}$ periodicity in the STM images, while the 5 × 5 periodicity appears relatively clearly at –2.0 V (Fig. 3(a)) and –1.5 V (Fig. 3(b)), where it can be seen in addition to the fundamental 1 × 1 periodicity. Also the 5 × 5 does however become less evident at higher bias voltages, with several complicated contrast patterns emerging at –1.0V (Fig. 3(c)), +1.0V (Fig. 3(d)) and +1.5V (Fig. 3(e)), although the fundamental 1 × 1 still remains clear. Finally, at the highest examined bias voltage of +2.0V (Fig. 3(f), even the 1 × 1 disappears, with the 5 × 5 somewhat recovering although with a contrast pattern that is markedly different from that observed at negative bias voltages.

Figures 4(a), 4(b) and 4(c) show STS spectra acquired on the $\sqrt{7} \times \sqrt{3}$ reconstruction, the In-TCNQ SMON(α), and the 5 × 5 reconstruction, respectively. The $\sqrt{7} \times \sqrt{3}$ spectrum in Fig. 4(a) shows one peak at approximately −0.7 eV attributed mainly to the In *p* orbitals in the filled-state region together with a second small shoulder peak at approximately +0.9 eV in the empty-state region.[21] Moreover, the spectrum shows a finite differential conductivity at the Fermi energy (0V), indicating that the $\sqrt{7} \times \sqrt{3}$ is electronically metallic.[21,33,34] The SMON(α) spectrum in Fig. 4(b) is characterized by two relatively broad peaks symmetrically centered around the Fermi energy at about −1.2 eV

and +1.2 eV, which are considered to be resonances arising from hole and electron attachments, respectively, to a singly occupied molecular orbital (SOMO) of the TCNQ molecule pinned at the Fermi energy.[17,29] Also this spectrum displays a finite differential conductivity at the Fermi energy, indicating that also the SMON(α) is electronically metallic. On the other hand, the 5 × 5 spectrum shows only one large peak of uncertain origin in the range between +0.8 eV and +1.6 eV, which might be responsible for the drastic change of the STM images between +1.5 eV and +2.0 eV (compare Figs. 3(e) and 3(f)). Interestingly, the differential conductivity at the Fermi energy becomes considerably smaller than those of the $\sqrt{7} \times \sqrt{3}$ and the SMON(α), indicating that the 5 × 5 reconstruction has a stronger insulating character (this is further supported by the I-V curves in Fig. S3 of the ESI†). This electronic property could be the reason for the neat HOMO-like appearance of isolated (and thus neutral) TCNQ molecule on the 5 × 5 reconstruction when imaged at a negative bias voltage (Fig. 1(d)); this is indeed not the case for neutral TCNQ molecules adsorbed on metallic Au(111),[20,35] but occurs for TCNQ molecules on graphene on metals, due to the electronically decoupling action of the graphene layer.[30]

In order to extend the 5 × 5 regions, we attempted to gradually increase the amount of adsorbed TCNQ by exposing the substrate to increasingly longer molecular doses. Fig. 5(a) shows a typical STM image after an extended TCNQ exposure. A terrace mostly with the $\sqrt{7} \times \sqrt{3}$ reconstruction can be seen at the center of the image, on which TCNQ molecules form regular arrangements. Figs. 5(b) and (c) show an enlarged STM image taken at similar location to 5(a). The former and the latter display the same image at different contrasts, in order to enhance the visibility of the molecular structures and of the reconstructions on the Si(111) surface, respectively. White solid and dashed parallelograms in Fig. 5(b) indicate unit cells of the $\sqrt{7} \times \sqrt{3}$ and the 5 × 5 reconstructions, respectively. The TCNQ molecules form regular arrangements also after these prolonged doses but their structure is different from that of the SMON(α) phase. Fig. 5(b) shows that the molecules still have a LUMO-like appearance when imaged at negative sample bias (indicating that they are negatively charged as is expected in SMONs) but that they pack parallel to each other instead of forming windmill arrangement. A molecular model overlaid on the STM image in Fig. 5(b) shows a good fit with the main (sub)molecular

features, proving that the TCNQ molecules still arrange into a SMON with In atoms, but that this is different from SMON(α). As a matter of fact, the SMON in Fig. 5(b) closely resembles the β phase of the Ni-TCNQ SMON formed on Ag(100),[12] of the Mn-TCNQ SMON on Ag(100)[12] and on Au(111),[14] of the Au-TCNQ SMON on Au(111),[20] and of the denser Ag-TCNQ SMON on Ag(111),[16] and will therefore be denoted as SMON(β) hereafter. Densities of both the TCNQ molecules and the metal centers are higher for the β phase than for the α phase. Interestingly, the surface reconstruction around the In-TCNQ SMON(β) is not the 5 × 5, but the $\sqrt{7} \times \sqrt{3}$ as shown in the lower right side of Fig. 5(c). Furthermore, at some locations, an incomplete 5 × 5 reconstruction could be observed (see, for example, the lower left side of Fig. 5(c)), which is considered to be intermediate step in structural phase transition between the 5 × 5 and the $\sqrt{7} \times \sqrt{3}$ reconstructions. Consequently, when the deposited amount of the TCNQ increased, the 5 × 5 regions extended first at the cost of the $\sqrt{7} \times \sqrt{3}$ regions but, before covering the whole surface, they started to shrink and, finally, disappeared, concomitantly with the SMON(α) changing to the SMON(β).

First-principles DFT calculations were performed to investigate the possible atomic arrangements of the In atoms in the $\sqrt{7} \times \sqrt{3}$ and the 5 × 5 reconstructions and to shed light onto the transition from one to the other. In our previous work,[21] we showed that "rect" is the most favorable configuration in the $\sqrt{7} \times \sqrt{3}$ reconstruction for an In coverage of 2.4 ML;[36] therefore, we used this configuration as our starting point. Since the 5 × 5 and the $\sqrt{7} \times \sqrt{3}$ are commensurate with each other (see Fig. 2), we used a (5 × 5) surface unit cell for both the 5 × 5 and the $\sqrt{7} \times \sqrt{3}$ reconstructions (as explained in the "Computational Methods"); thus, an In coverage of 2.4 ML corresponds to two layers with 30 In atoms in each layer. Motivated by the experimental STM images in Figs. 3(a) and 3(b), which show a triangular motif, we also considered several configurations in which the In atoms of the topmost layer were initially arranged within the rhombic supercell in two triangles, (denoted as "triang" configurations hereafter), in addition to the "rect" configuration. It is noted that although we investigated several "triang" configurations (not shown here), we selected only "triang-1" and "triang-2" because (i)

"triang-1" is the configuration with more similarities to the experimental STM images and (ii) "triang-2" was found to be the energetically most favorable "triang" configuration (see the atomic arrangement of the "rect" and the two "triang" configurations in Figs. 6and S4 of the ESI†). For 2.4 ML coverage (double layer with 30+30 In atoms), we found that "rect" is the most favorable configuration, with formation energy E_f at least 0.3 eV lower than the "triang" configurations (see Fig. 7).

Since we believe that small amount of In atoms must be taken from the $\sqrt{7} \times \sqrt{3}$ reconstruction to form the In-TCNQ SMON(α), we also investigated the atomic structure and stability of the "rect" and the "triang" configurations for slightly lower In coverage: in particular we considered 2.36 and 2.32 ML coverages, which are equivalent to a double In layer with 30+29 and 30+28 In atoms, respectively. In the "rect" configuration, the 29 or 28 In atoms in the topmost layer correspond to a single or double vacancy, respectively, in an ordered lattice (see Figs. 8 and S5 of the ESI†). As can be seen in Fig. 7, the "rect" configuration becomes less favorable with decreasing In-coverage, while the "triang" configurations become more favorable; in particular, at 2.32-ML coverage the energy of the two configurations is essentially identical, with "triang-2" being just ~0.02 eV more favorable than "rect". It is worth noting that reducing the number of In atoms in the topmost layer brings the atomic density close to the value in bulk indium. In the (100) plane of face-centered tetragonal bulk indium, the planar atomic density is 8.79 nm^{-2}, while it is 9.40, 9.09, and 8.77 nm^{-2} in the reconstructed top layer with 30, 29 and 28 In atoms, respectively. The simulated STM images (see Fig. S6 of the ESI†), obtained using the Tersoff-Hamann approach[37] as described in Ref.,[21] do not resemble the experimental STM images displayed in Fig. 3 very much. However, both the simulated STM images of the two "triang" configurations and the experimental STM images show a triangular symmetry, while the simulated STM image of the "rect" configuration does not show it at all. Since several atomic configurations were found to be very close in energy, it is conceivable that the experimentally observed reconstruction is characterized by the coexistence of several atomic structures. The associated contribution from configurational entropy could further help to lower the free energy at finite temperature.

It is noted that the global minimum of the formation energy at 2.4 ML is predicted to be the "rect" structure with a $\sqrt{7} \times \sqrt{3}$ symmetry. The 5 × 5 is experimentally observed close to the SMON(α), which causes the removal of a small amount of indium atoms from the surface and might also have a possible local stabilizing effect which is not considered in our calculations. On the other hand, the development of the SMON(β) and

the concomitant disappearance of the 5 × 5 reconstruction is much less clear. In fact, the SMON(β) should incorporate even more In atoms than the SMON(α) and, in a first approximation, one would expect its formation to promote the extension of the 5 × 5 regions, instead of their shrinking. A wider set of (possibly coexisting) surface structures than those considered theoretically and a strong influence of the SMONs on the surface energetics might be at the origin of the complex behavior that marks the experimental results. However, this indicates that the formation mechanism of the experimentally observed 5 × 5 reconstruction is still not fully clear.

Finally, we investigated the electronic properties of the "rect" and the two "triang" configurations and how they are affected by the reduction of the In coverage. As shown in Fig. 9, by reducing the In coverage to 2.32 ML, the projected density of states (PDOS) of the In layer around the Fermi energy is reduced in all three configurations when compared to the "rect" configuration for 2.4 ML. This is in line with the experimental finding that the 5 × 5 reconstruction is more insulating than the $\sqrt{7} \times \sqrt{3}$ reconstruction. The reduced DOS of the In layer around the Fermi energy suggests that the STM images of the 5 × 5 reconstruction might not reflect the In layers, but instead mainly the Si substrate below them. In Bardeen–Cooper–Schrieffer theory of superconductivity, the T_c depends sensitively on the electronic DOS at the Fermi energy, as higher DOS implies higher T_c. Because the 5 × 5 reconstruction has a reduced DOS at the Fermi energy compared to the $\sqrt{7} \times \sqrt{3}$ reconstruction, the 5 × 5 is expected to have a lower T_c than the $\sqrt{7} \times \sqrt{3}$. PDOS of Si slab and total DOS of the "rect" and the two "triang" configurations are shown in Fig. S7 of the ESI†.

Conclusions

In conclusion, we have investigated the adsorption of TCNQ on the Si(111)-$\sqrt{7} \times \sqrt{3}$-In surface by STM and STS. We found that In-TCNQ surface metal-organic networks formed and that this caused a surface structural phase transition from the $\sqrt{7} \times \sqrt{3}$ to the

previously unknown 5 × 5 reconstruction. The 5 × 5 reconstruction is regarded as a superstructure of the $\sqrt{7} \times \sqrt{3}$ reconstruction, and STS spectra show that it has more insulating character than the $\sqrt{7} \times \sqrt{3}$ reconstruction. DFT calculations suggest that the structural phase transition is probably driven by a slight reduction of the coverage of the topmost indium layer that provides indium atoms to be incorporated into the In-TCNQ two-dimensional networks.

Conflicts of interest

There are no conflicts to declare

Acknowledgements

This work was partly supported by funding from the Central Research Institute of Fukuoka University (Grant no. 185008) and funding by JSPS KAKENHI (Grant no. 15K04630). Financial support within SFB 1242 "Non-equilibrium dynamics of condensed matter in the time domain" funded by Deutsche Forschungsgemeinschaft (DFG), project number 278162697, is gratefully acknowledged by JMM and PK. JMM and PK also gratefully acknowledge the computing time granted by the Center for Computational Sciences and Simulation (CCSS) of the University of Duisburg-Essen and provided on the supercomputer magnitUDE (DFG Grants No. INST 20876/209-1 FUGG and No. INST 20876/243-1 FUGG) at the Zentrum für Informations- und Mediendienste (ZIM).

Notes and references

1 T. Zhang, P. Cheng, W. -J. Li, Y. -J. Sun, G. Wang, X. -G. Zhu, K. He, L. Wang, X. Ma, X. Chen, Y. Wang, Y. Liu, H. -Q. Lin, J. -F. Jia, and Q.-K. Xue, Nature Phys. 2010, **6**, 104.

2 T. Uchihashi, P. Mishra, M. Aono, and T. Nakayama, Phys. Rev. Lett. 2011, **107**, 207001.

3 T. Uchihashi, P. Mishra, and T. Nakayama, Nanoscale Res. Lett. 2013, **8**, 167.

4 M. Yamada, T. Hirahara, and S. Hasegawa, Phys. Rev. Lett. 2013, **110**, 237001.

5 S. Yoshizawa, H. Kim, T. Kawakami, Y. Nagai, T. Nakayama, X. Hu, Y. Hasegawa, and T. Uchihashi, Phys. Rev. Lett. 2014, **113**, 247004.
6 S. Yoshizawa, E. Minamitani, S. Vijayaraghavan, P. Mishra, Y. Takagi, T. Yokoyama, H. Oba, J. Nitta, K. Sakamoto, S. Watanabe, T. Nakayama, and T. Uchihashi, Nano Lett. 2017, **17**, 2287.
7 N. Sumi, Y. Yamada, M. Sasaki, R. Arafune, N. Takagi, S. Yoshizawa, T. Uchihashi, J. Phys. Chem. C 2019, **123**, 8951.
8 L. Dong, Z. A. Gao, and N. Lin, Prog. Surf. Sci. 2016, **91**, 101.
9 R. Robson, Dalton Trans., 2008, 5113.
10 M. Li, D. Li, M. O'Keeffe, and O. M. Yaghi, Chem. Rev. 2014, **114**, 1343.
11 J. Ferraris, D. O. Cowan, V. Walatka, and J. H. Perlstein, J. Am. Chem. Soc. 1973, **95**, 948.
12 T. -C. Tseng, N. Abdurakhmanova, S. Stepanow, and K. Kern, J. Phys. Chem. C 2011, **115**, 10211.
13 N. Abdurakhmanova, T. -C. Tseng, A. Langner, C. S. Kley, V. Sessi, S. Stepanow, and K. Kern, Phys. Rev. Lett. 2013, **110**, 027202.
14 M. N. Faraggi, V. N. Golovach, S. Stepanow, T. -C. Tseng, N. Abdurakhmanova, C. S. Kley, A. Langner, V. Sessi, K. Kern, and A. Arnau, J. Phys. Chem. C 2015, **119**, 547.
15 N. Abdurakhmanova, A. Floris, T. -C. Tseng, A. Comisso, S. Stepanow, A. De Vita, and K. Kern, Nat. Commun. 2012, **3**, 940.
16 C. Wackerlin, C. Iacovita, D. Chylarecka, P. Fesser, T. A. Jung, and N. Ballav, Chem. Commun. 2011, **47**, 9146.
17 T. R. Umbach, I. Fernández-Torrente, M. Ruby, F. Schulz, C. Lotze, R. Rurali, M. Persson, J. I. Pascual, and K. J. Franke, New J. Phys. 2013, **15**, 083048.
18 P. J. Blowey, L. A. Rochford, D. A. Duncan, D. A. Warr, T. -L. Lee, D. P. Woodruff, and G. Costantini, Faraday Discuss. 2017, **204**, 97.
19 P. J. Blowey, S. Velari, L. A. Rochford, D. A. Duncan, D. A. Warr, T.-L. Lee, A. De Vita, G. Costantini, and D. P. Woodruff, Nanoscale 2018, **10**, 14984.
20 A. Della Pia, M. Riello, D. Stassen, T. S. Jones, D. Bonifazi, A. De Vita, and G. Costantini, Nanoscale 2016, **8**, 19004.
21 T. Suzuki, J. Lawrence, M. Walker, J. M. Morbec, P. Blowey, K. Yagyu, P. Kratzer, and G. Costantini, Phys. Rev. B 2017, **96**, 035412.
22 W. Kohn and L. J. Sham, Phys. Rev. 1965, **140**, A1133.
23 V. Blum, R. Gehrke, F. Hanke, P. Havu, V. Havu, X. Ren, K. Reuter, and M. Scheffler, Comput. Phys. Commun. 2009, **180**, 2175.

24 J. P. Perdew, K. Burke, and M. Ernzerhof, Phys. Rev. Lett. 1996, **77**, 3865.
25 H. J. Monkhorst and J. D. Pack, Phys. Rev. B 1976, **13**, 5188.
26 D. Shin, J. Woo, Y. Jeon, H. Shim, and G. Lee, J. Korean Phys. Soc. 2015, **67**, 1192.
27 M. Kawaji, S. Baba, and A. Kinbara, Appl. Phys. Lett. 1979, **34**, 748.
28 J. Kraft, M. G. Ramsey, and F. P. Netzer, Phys. Rev. B 1997, **55**, 5384.
29 M. Garnica, D. Stradi, S. Barja, F. Calleja, C. Díaz, M. Alcamí, N. Martín, A. L. Vázquez de Parga, F. Martín, and R. Miranda, Nature Phys. 2013, **9**, 368.
30 D. Maccariello, M. Garnica, M. A. Niño, C. Navío, P. Perna, S. Barja, A. L. Vázquez de Parga, R. Miranda, Chem. Mater. 2014, **26**, 2883.
31 R. Precht, R. Hausbrand, and W. Jaegermann, Phys. Chem. Chem. Phys. 2015, **17**, 6588.
32 R. Precht, S. Stolz, E. Mankel, T. Mayer, W. Jaegermann, and R. Hausbrand, Phys. Chem. Chem. Phys. 2016, **18**, 3056.
33 E. Rotenberg, H. Koh, K. Rossnagel, H. W. Yeom, J. Schäfer, B. Krenzer, M. P. Rocha, and S. D. Kevan, Phys. Rev. Lett. 2003, **91**, 246404.
34 S. Yamazaki, Y. Hosomura, I. Matsuda, R. Hobara, T. Eguchi, Y. Hasegawa, and S. Hasegawa, Phys. Rev. Lett. 2011, **106**, 116802.
35 I. F. Torrente, K. J. Franke, J. I. Pascual, Int. J. Mass Spectrom. 2008, **277**, 269.
36 J. W. Park, and M. H. Kang, Phys. Rev. B 2015, **92**, 045306.
37 J. Tersoff and D. R. Hamann, Phys. Rev. Lett. 1983, **50**, 1998; Phys. Rev. B 1985, **31**, 805.

Figure 1 Typical STM images (a) before and (b) after the TCNQ adsorption on the Si(111)-$\sqrt{7} \times \sqrt{3}$-In surface. Enlarged STM images of the SMON(α) and the 5 × 5 reconstruction are shown in (c) and (d), respectively. High-contrast reproductions of the regions highlighted by white dotted contours are shown as insets in (c) and (d), together with a molecular model of the In-TCNQ SMON(α) structure in (c). A fast Fourier transform pattern of the 5 × 5 reconstruction is shown in the inset of (d). Image sizes are (a,b) 73 × 73 nm^2, (c) 9 × 9 nm^2 and (d) 18 × 18 nm^2. Bias voltages and tunneling currents are (a) +2.0V, 0.2 nA, and (b - d) –2.0 V, 0.1 nA, respectively.

Figure 2 Schematic drawing of the bulk terminated Si(111) surface with the 5 × 5 and the $\sqrt{7} \times \sqrt{3}$ periodicities indicated by red and blue unit cells, respectively.

Figure 3 STM images of the 5 × 5 reconstruction acquired at the same sample position with six different sample-bias voltages. Image size is 8 × 8 nm^2. Tunneling current is 0.1 nA.

Figure 4 STS spectra acquired on (a) the $\sqrt{7} \times \sqrt{3}$ reconstruction,[21] (b) the In-TCNQ SMON(α) and (c) the 5 × 5 reconstruction.

Figure 5 (a) Typical STM image of the SMON(β) formed after a prolonged TCNQ dose. (b) and (c) display the same STM image taken at similar location to (a) at different contrasts in order to enhance the visibility of the molecular structures and of the Si(111) reconstructions, respectively. Image sizes are (a) 73 × 73 nm^2 and (b,c) 18 × 11 nm^2. Bias voltage and tunneling current are (a) –2.5 V, 0.1 nA and (b,c) –2.5 V, 0.1 nA.

Figure 6 Top and side views (in BallStick display mode) of the "rect" and the two "triang" configurations with 2.4 ML In coverage. Yellow spheres represent the Si atoms; bright/dark gray spheres represent top-/bottom-layer In atoms; red lines indicate the 5 × 5 surface unit cell. Relative total energies (ΔE) with respect to the "rect" configuration are shown at the top of each figure.

Figure 7 Calculated formation energies of the "rect" and the "triang" configurations as function of the In coverage. See Figs. 6 and 8 for the atomic arrangement of the "rect" and the two "triang" configurations.

Figure 8 Top and side views (in BallStick display mode) of the "rect" and the two "triang" configurations with 2.32 ML In coverage. Yellow spheres represent the Si atoms; bright/dark gray spheres represent top-/bottom-layer In atoms; red lines indicate the 5 × 5 surface unit cell. Relative total energies (ΔE) with respect to the "rect" configuration are shown at the top of each figure.

Figure 9 Projected density of states (PDOS) of In layers for the (a) "rect", (b) "triang-1" and (c) "triang-2" configurations with In-coverage of 2.4 and 2.32 ML.

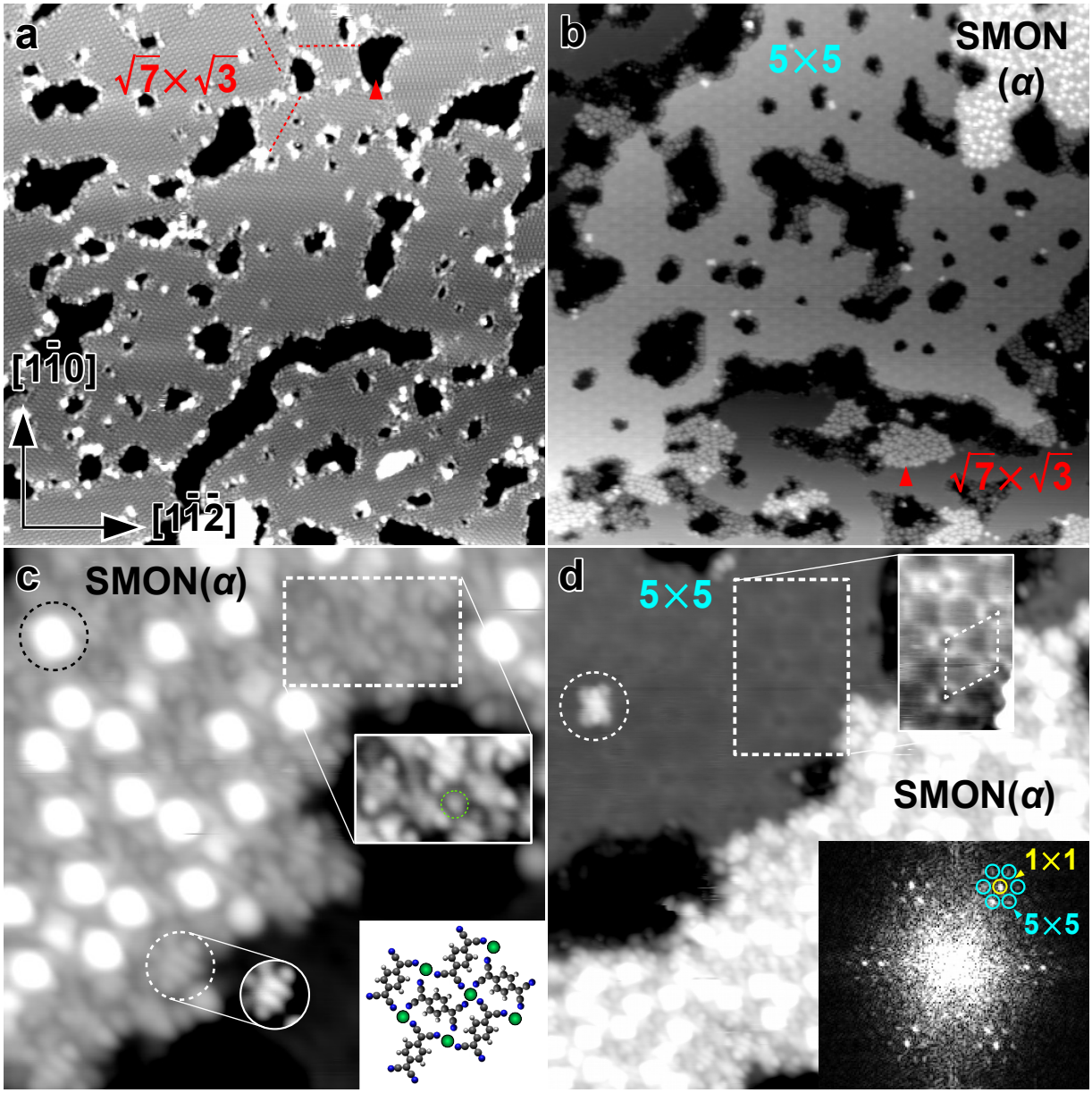

Figure 1 Suzuki, et.al.

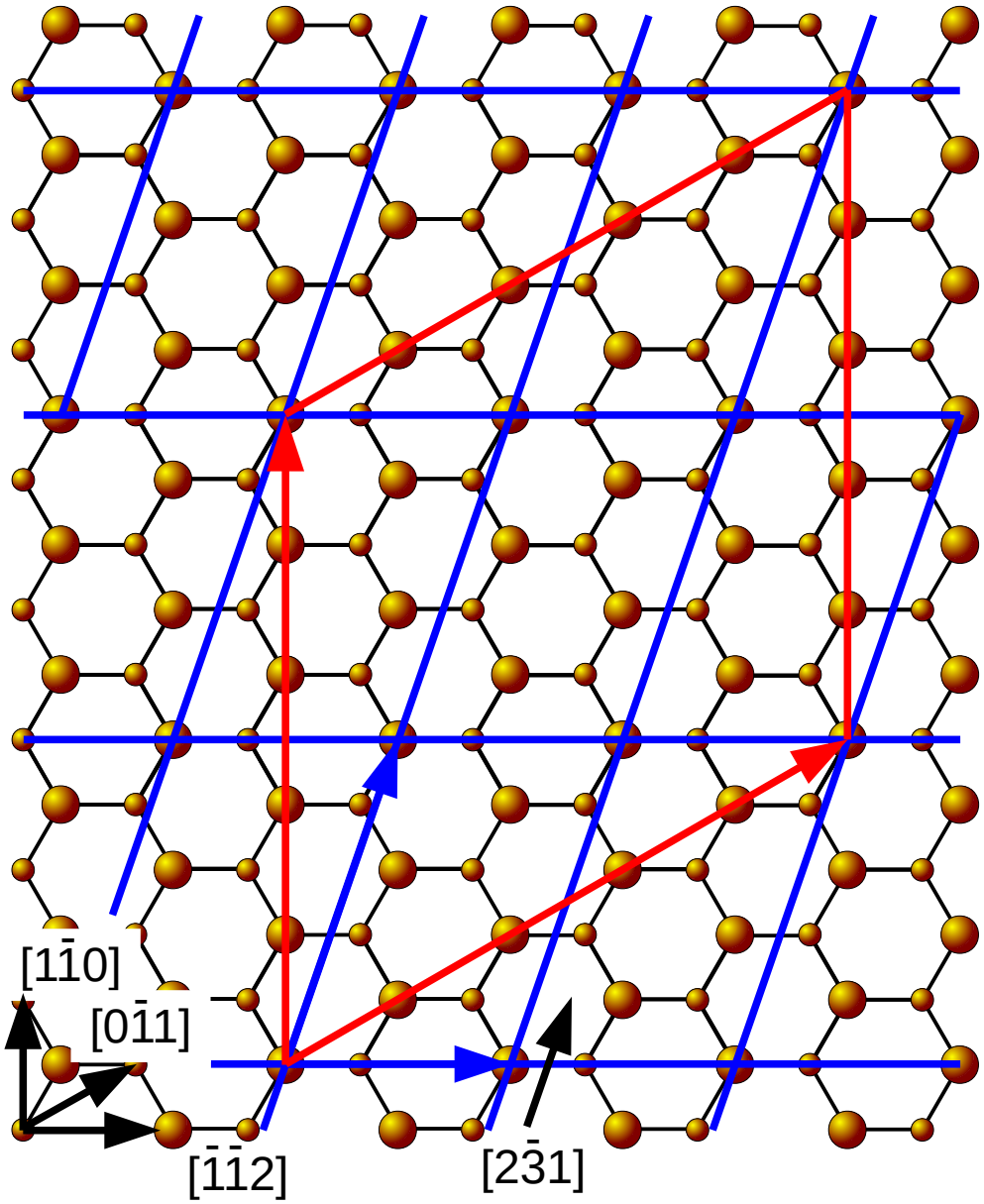

Figure 2 Suzuki, et.al.

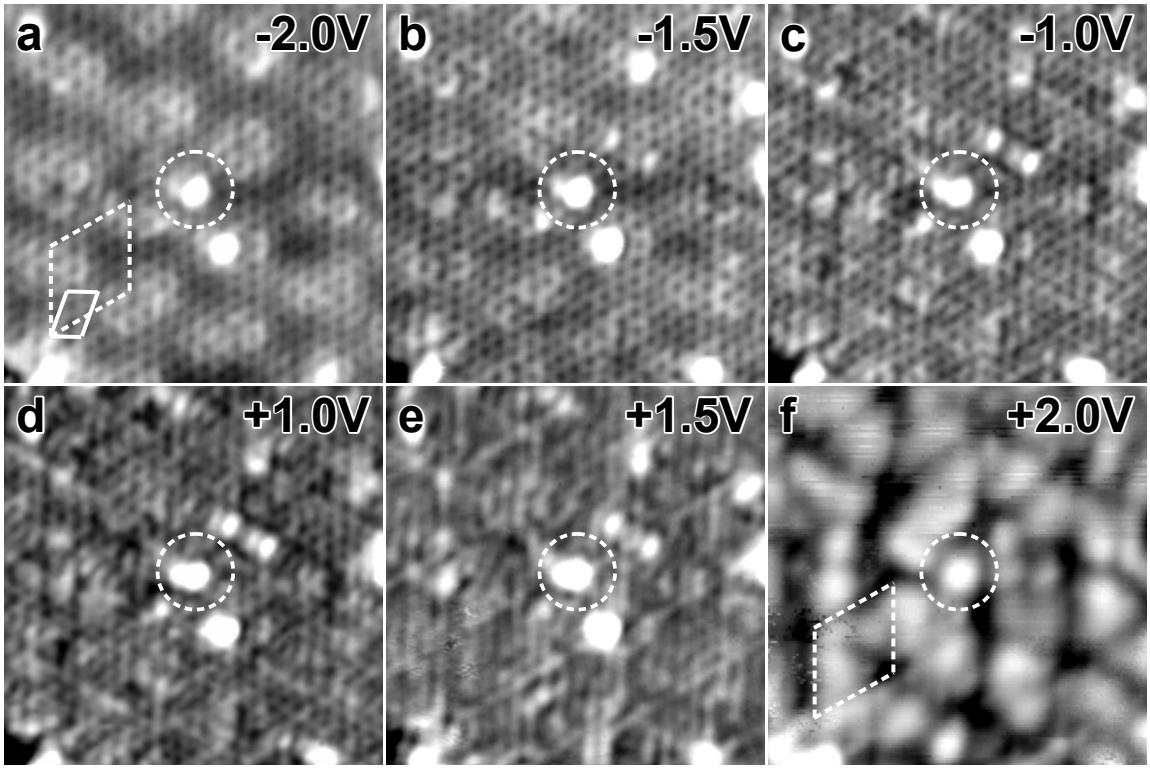

Figure 3 Suzuki, et.al.

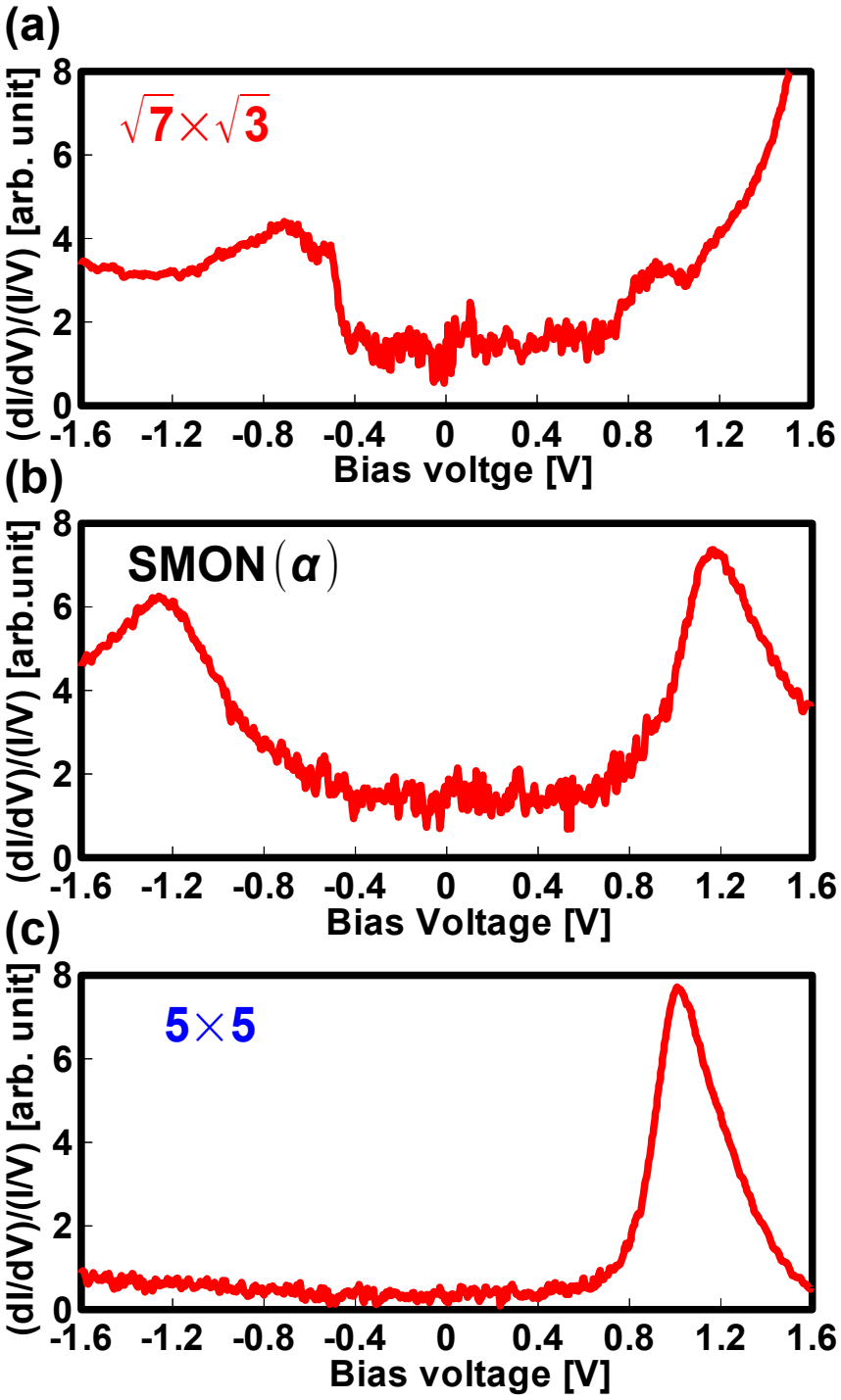

Figure 4 Suzuki, et.al.

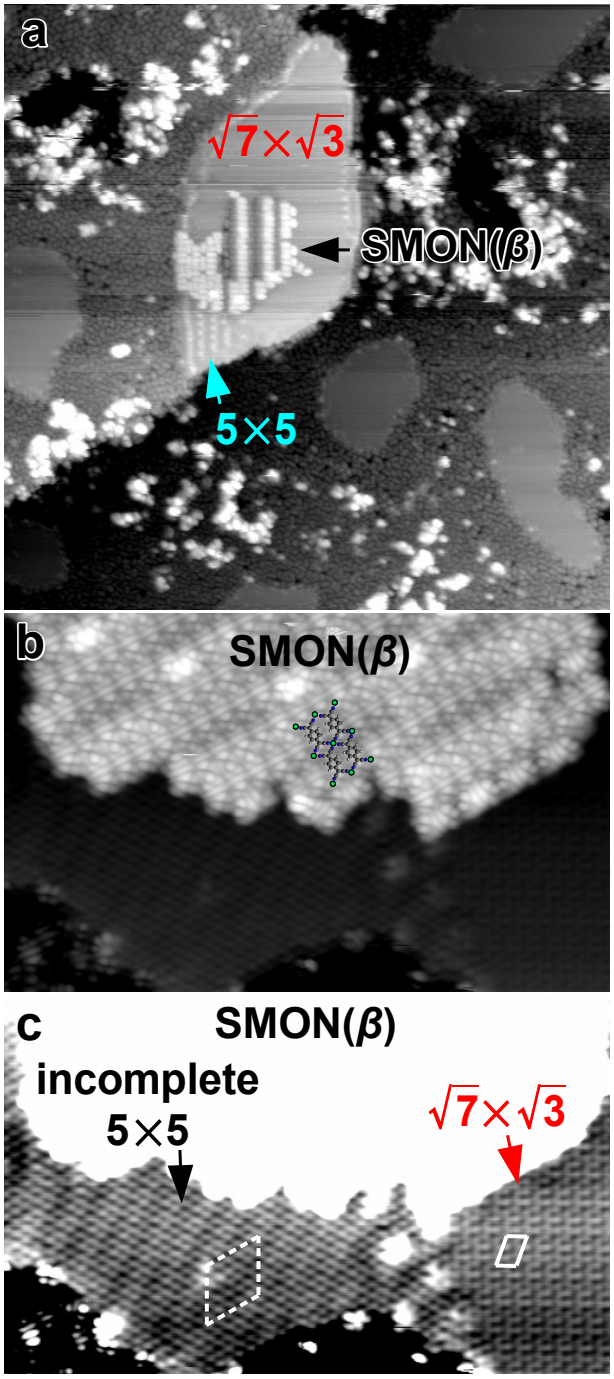

Figure 5 Suzuki, et.al.

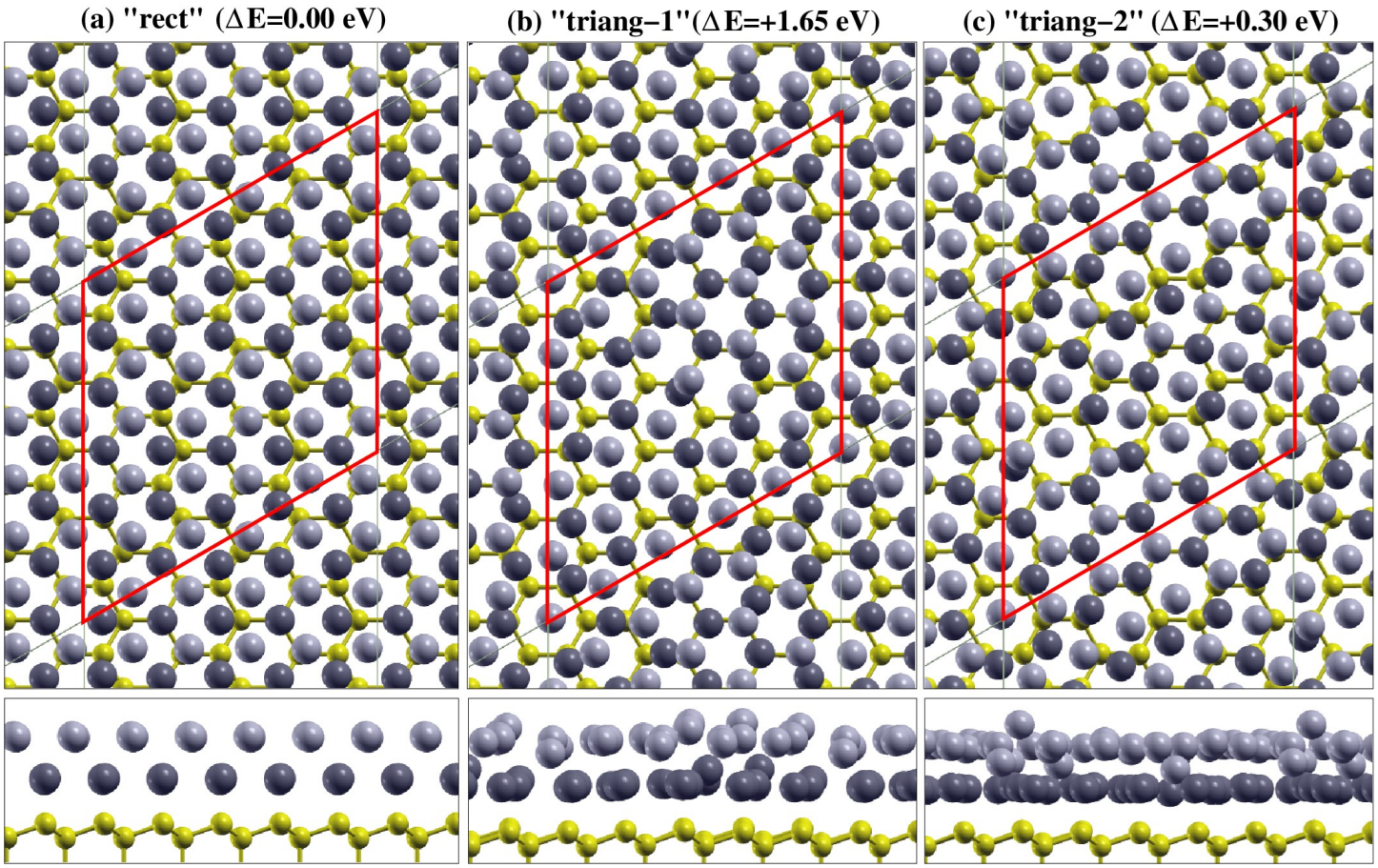

Figure 6 Suzuki, et.al.

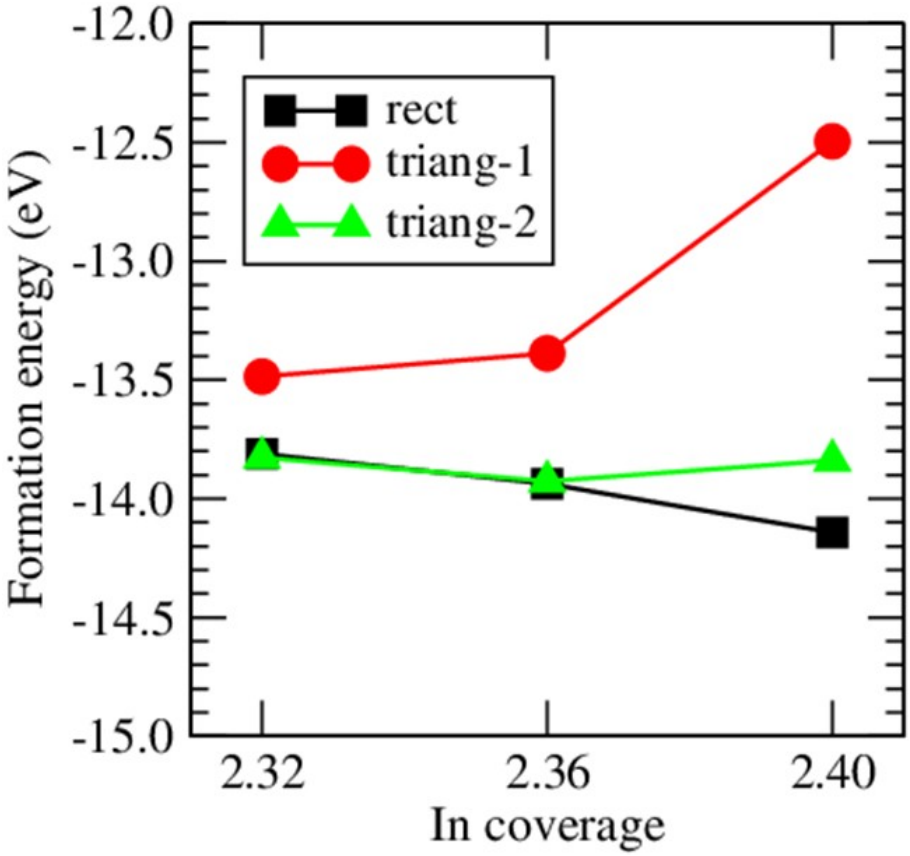

Figure 7 Suzuki, et.al.

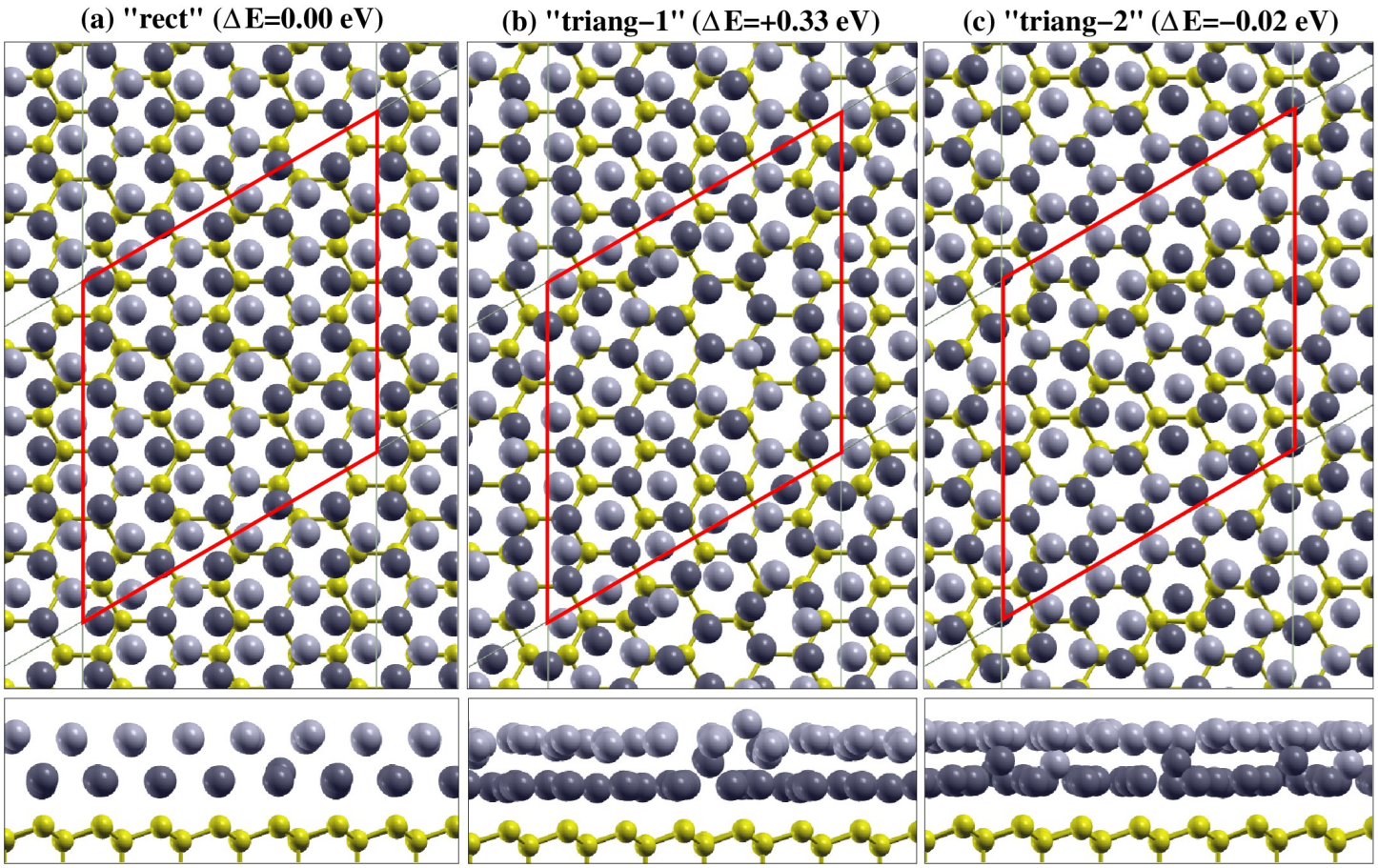

Figure 8 Suzuki, et.al.

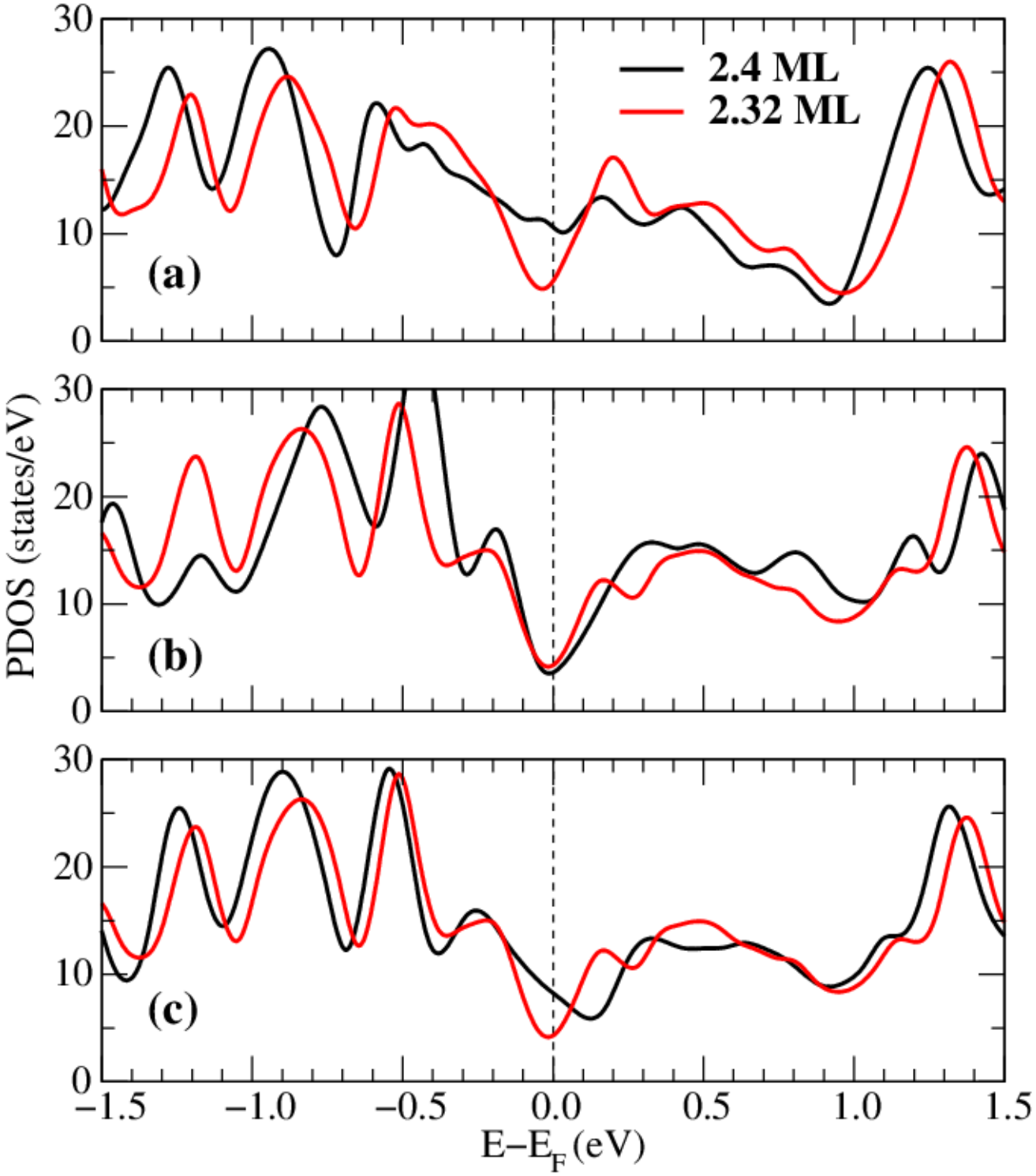

Figure 9 Suzuki, et.al.